Inorganic Chemistry

including bioinorganic chemistry

September 15, 2014
Volume 53, Number 18
pubs.acs.org/IC

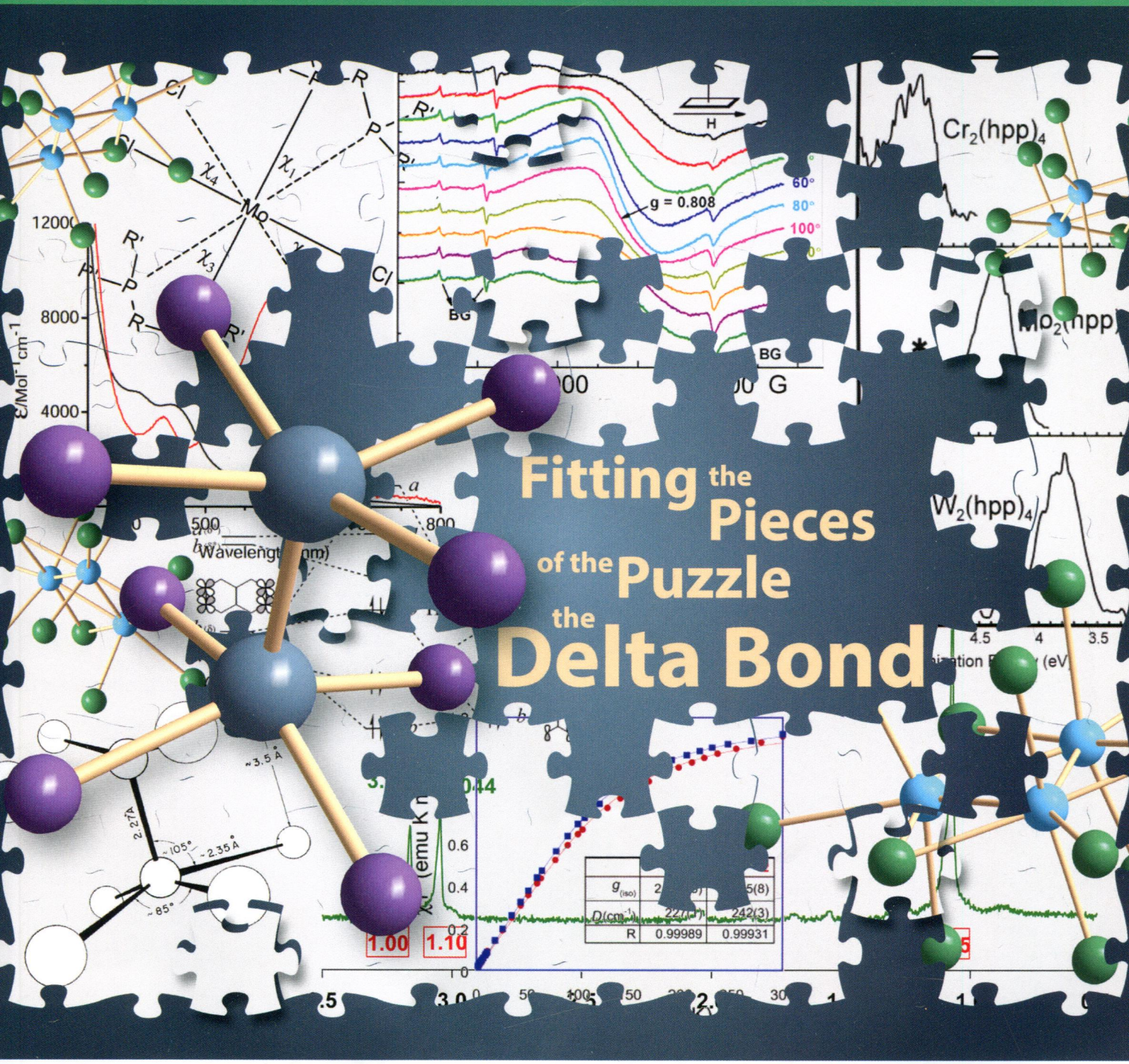

ACS Publications
Most Trusted. Most Cited. Most Read.

www.acs.org

Inorganic Chemistry

SEPTEMBER 15, 2014
VOLUME 53 ISSUE 18

INOCAJ 53(18) 9441−9982 (2014)
ISSN 0020-1669
Registered in the U.S. Patent and Trademark Office

ON THE COVER: The first description of a quadruple bond and its characteristic delta component, published by Cotton et al. 50 years ago (*Science* **1964**, *145*, 1305), launched a field of research that still occupies a place in the vanguard of Inorganic Chemistry. A Viewpoint article in this issue gives an account of the original discovery and an overview of how synthesis, structure, and many other forms of characterization fit together to give an integrated picture of the delta bond. See L. R. Falvello, B. M. Foxman, and C. A. Murillo, p 9441.

Viewpoint

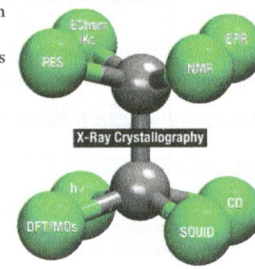

Communications

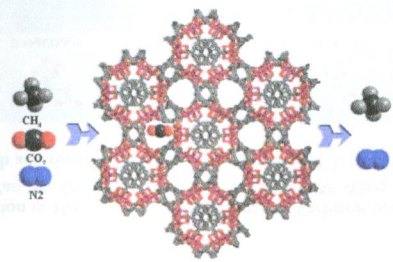

9460 S dx.doi.org/10.1021/ic5015863

Molybdenum Site Structure of MOSC Family Proteins

Logan J. Giles, Christian Ruppelt, Jing Yang, Ralf R. Mendel,* Florian Bittner,* and Martin L. Kirk*

Mo K-edge X-ray absorption spectroscopy has been used to probe the MOSC family proteins pmARC-1 and HMCS-CT. X-ray absorption near-edge structure spectra show that pmARC-1 is more oxidized than HMCS-CT, suggesting Mo^{VI} and Mo^{IV} oxidation states, respectively. Extended X-ray absorption fine structure analysis reveals a dioxo structure for pmARC-1 that is similar to oxidized sulfite oxidase. HMCS-CT possesses a single terminal oxo, dithiolene, and coordinated water with either a coordinated cysteine or cysteine persulfide. These data provide a foundation for understanding the oxygen-atom-transfer reactivity in pmARC and the sulfuration mechanism of XO family enzymes mediated by HMCS-CT.

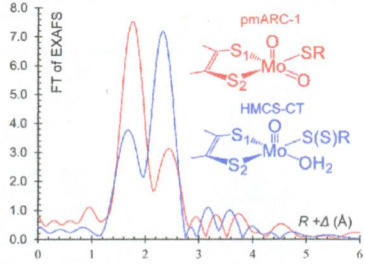

9463 S dx.doi.org/10.1021/ic501901n

Carbon Dioxide Hydrosilylation Promoted by Cobalt Pincer Complexes

Margaret L. Scheuermann, Scott P. Semproni, Iraklis Pappas, and Paul J. Chirik*

The addition of CO_2 to (^{tBu}PNP)CoH [^{tBu}PNP = 2,6-bis(di-*tert*-butylphosphinomethyl)pyridine] resulted in rapid insertion into the Co−H bond to form the corresponding κ^1-formate complex, which has been structurally characterized. The treatment of (^{tBu}PNP)CoH with $PhSiH_3$ resulted in oxidative addition to form *trans*-(^{tBu}PNP)Co(H)$_2$(SiH_2Ph), a compound that undergoes rapid exchange with excess free silane. In the presence of 0.5 mol % (^{tBu}PNP)CoH, the catalytic hydrosilylation of CO_2 with $PhSiH_3$ to a mixture of silyl formates, bis(silyl)acetyls, and silyl ethers has been observed.

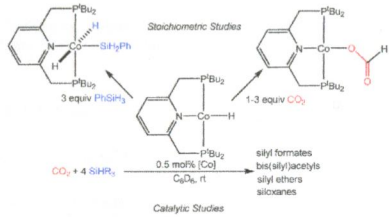

9466 dx.doi.org/10.1021/ic500202g

Theoretical Insights on the Interaction of Uranium with Amidoxime and Carboxyl Groups

Cong-Zhi Wang, Jian-Hui Lan, Qun-Yan Wu, Qiong Luo, Yu-Liang Zhao, Xiang-Ke Wang, Zhi-Fang Chai,* and Wei-Qun Shi*

The uranyl extraction complexes with adsorbents containing amidoximate (AO^-), glutarimidedioximate (HA^-), and carboxyl (Ac^-) groups.

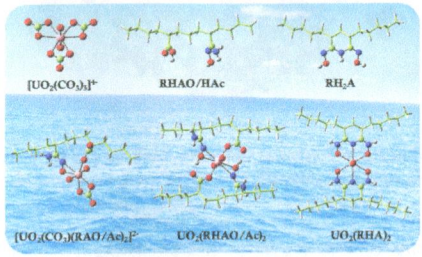

9477 dx.doi.org/10.1021/ic5004484

Structural and Thermodynamic Study of the Complexes of Nd(III) with *N,N,N′,N′*-Tetramethyl-3-oxa-glutaramide and the Acid Analogues

Guoxin Tian, Simon J. Teat,* and Linfeng Rao*

Neodymium(III) forms tridentate complexes with three structurally related carboxylate-amide ligands in aqueous solutions. Thermodynamic data show that the complexation is driven by both enthalpy and entropy and that the substitution of a carboxylate group with an amide group on the ligands enhances the enthalpy-driven force but weakens the entropy-driven force of the complexation.

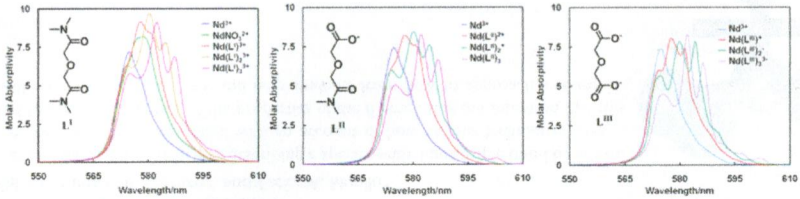

9486 dx.doi.org/10.1021/ic500442k

pH-Controlled and Sulfite Anion-Directed Assembly of a Family of Cerium(III)-Containing Polyoxotungstates Clusters

Wei-Chao Chen, Xin-Long Wang,* Yan-Qing Jiao, Peng Huang, En-Long Zhou, Zhong-Min Su,* and Kui-Zhan Shao

A versatile one-pot strategy was employed to synthesize five cerium(III)-containing polyoxotungstate nanoclusters through pH-controlled and sulfite anion-directed assembly: $\{Ce_2W_{22}\}$ (**1**) at pH 5.0; $\{Ce_4W_{44}\}$ (**2**) at pH 4.5; $\{Ce_2W_{28}\}$ (**3**) at pH 2.8−3.3; the unique sulfur-containing polyoxotungstate cluster $\{Ce_2S_3W_{28}\}$ (**4**) at pH 2.5; the largest lanthanide-containing iso-polyoxotungstates $\{Ce_2W_{36}\}_2$ (**5**) at pH 1.5. The compounds were characterized by single-crystal X-ray structure analysis, IR spectroscopy, thermogravimetric analysis, X-ray photoelectron spectroscopy, and electrospray ionization mass spectrometry. Moreover, their electrochemical properties were investigated.

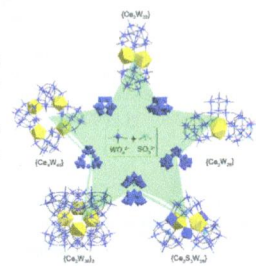

9498 (S) dx.doi.org/10.1021/ic5005837

Enhanced Luminescence in Ln^{3+}-Doped Y_2WO_6 (Sm, Eu, Dy) 3D Microstructures through Gd^{3+} Codoping

Anna M. Kaczmarek,* Kristof Van Hecke, and Rik Van Deun*

A detailed investigation of the photoluminescence properties of Sm^{3+}-, Eu^{3+}-, and Dy^{3+}-doped Y_2WO_6 3D microspheres built from nanosized building blocks was carried out. An enhancement in luminescence properties was observed when Gd^{3+} ions were additionally incorporated into the materials. This gave rise to high quantum yield values, up to 79% for the most efficient system. Several white-light-emitting samples were obtained.

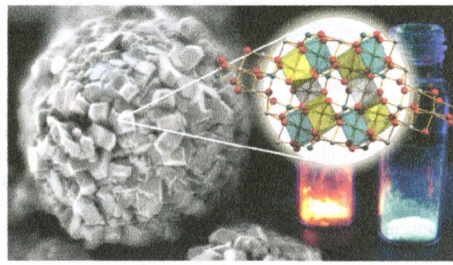

9509 (S) dx.doi.org/10.1021/ic500607a

Synthesis and Characterization of Amine-Functionalized Mixed-Ligand Metal–Organic Frameworks of UiO-66 Topology

Sachin M. Chavan,* Greig C. Shearer, Stian Svelle, Unni Olsbye, Francesca Bonino, Jayashree Ethiraj, Karl Petter Lillerud, and Silvia Bordiga*

A series of amine functionalized mixed-linker metal–organic frameworks (MOFs) of UiO-66 topology has been prepared and thoroughly characterized by TGA, PXRD, UV-vis, and FTIR spectroscopy with the aim of elucidating the effect that varying degrees of amine functionalization has on the stability (thermal and chemical) and porosity of the framework. This work includes the first application of UV-vis spectroscopy in the quantification of ABDC in mixed-linker MOFs.

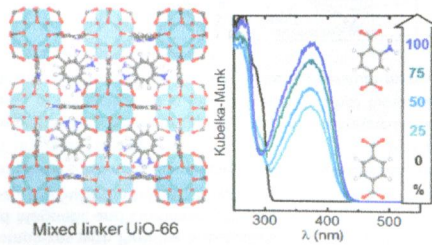

9516 dx.doi.org/10.1021/ic500646r

Pt(II) Bipyridyl Complexes Bearing Substituted Fluorenyl Motif on the Bipyridyl and Acetylide Ligands: Synthesis, Photophysics, and Reverse Saturable Absorption

Rui Liu, Yuhao Li, Jin Chang, Eric R. Waclawik, and Wenfang Sun*

The synthesis, photophysics, reverse saturable absorption, and the influence of the substituent at the bipyridyl and acetylide ligands on the nature of the excited states of a series of diimine Pt(II) complexes (**Pt-1**–**Pt-8**) were systematically investigated. **Pt-1**, **Pt-2**, **Pt-4**, and **Pt-5** exhibit strong reverse saturable absorption at 532 nm for ns laser pulses.

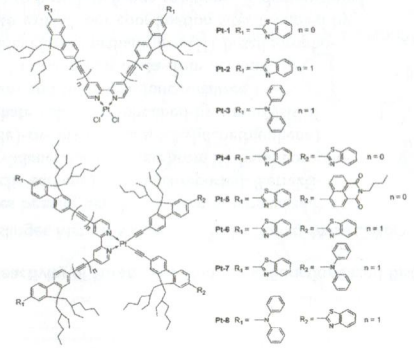

9531 dx.doi.org/10.1021/ic500681k

New Insight into Self-Irradiation Effects on Local and Long-Range Structure of Uranium–Americium Mixed Oxides (through XAS and XRD)

Florent Lebreton, Philippe M. Martin, Denis Horlait, René Bès, Andreas C. Scheinost, Andre Rossberg, Thibaud Delahaye,* and Philippe Blanchart

^{241}Am-induced self-irradiation effects on local and long-range structures were studied using XRD and XAS in 3- to 4-year-old U–Am mixed-oxide compounds stored under ambient conditions. After a first increase of both lattice volume and structural disorder, a steady state is reached and no further evolution is observed. The fluorite structure withstands the α-self-irradiation with no significant damage, through defect recombinations in low-ordered domains.

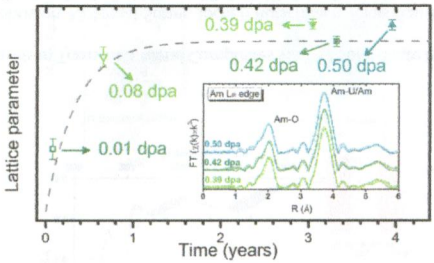

9541 dx.doi.org/10.1021/ic500748c

Crystal Structure, Electronic Structure, and Photoluminescence Properties of $La_3BW_{1-x}Mo_xO_9:Eu^{3+}$ Red Phosphor

Jinping Huang,* Binghu Hou, Hongya Ling, Jie Liu, and Xibin Yu

The $La_3BW_{1-x}Mo_xO_9:Eu^{3+}$ series red phosphors have been prepared. Mo^{6+} ions are incorporated into the lattice. The characteristic sharp lines of the excitation spectra join the ligand-to-metal charge transfer (LMCT) band into a broad band. The emission under a near-UV excitation is prominently enhanced. The relationships of the photoluminescence and the crystal structure and electronic structure are studied.

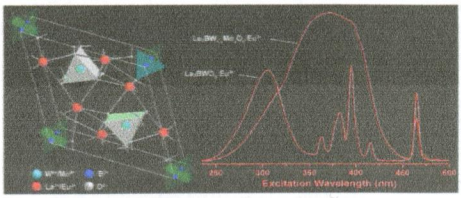

9548 dx.doi.org/10.1021/ic500779y

Terbium(III) and Yttrium(III) Complexes with Pyridine-Substituted Nitronyl Nitroxide Radical and Different β-Diketonate Ligands. Crystal Structures and Magnetic and Luminescence Properties

Anthony Lannes, Mourad Intissar, Yan Suffren, Christian Reber,* and Dominique Luneau*

Complexes of the nitronyl nitroxide free radical 2-(2-pyridyl)-4,4,5,5-tetramethylimidazoline-3-oxyl-1-oxide (NIT2Py) with general formulas $[M(acac)_3NIT2Py]$ and $[M(hfac)_3NIT2Py]$ ($M = Tb^{3+}$, Y^{3+}; acac = acetylacetonate; hfac = hexafluoroacetylacetonate) were synthesized, and their crystal structures determined. Magnetic studies reveal that the terbium compounds exhibit slow relaxation of magnetization at low temperature, while luminescence spectra of all compounds show resolved vibronic structure with the main interval decreasing as the temperature increases despite constant experimental Raman frequencies.

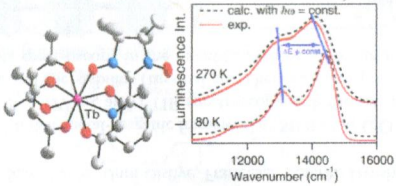

9561 dx.doi.org/10.1021/ic500854k

New Perspective in Garnet Phosphor: Low Temperature Synthesis, Nanostructures, and Observation of Multimodal Luminescence

Kavita Mishra, Sunil Kumar Singh,* Akhilesh Kumar Singh, Monika Rai, Bipin Kumar Gupta, and Shyam Bahadur Rai

Multimode phosphors possessing upconversion (UC), quantum cutting (QC), and downshifting (DS) emission, which has been developed by a facile solution combustion method, is demonstrated. The host and dopant show a broad excitation range of 250−500 nm; the discrete emission is obtained in the entire visible region through DS and QC processes. IR radiation is converted to discrete visible emission via a frequency UC process. The existence of this multimode emission could open new applications for garnet phosphors.

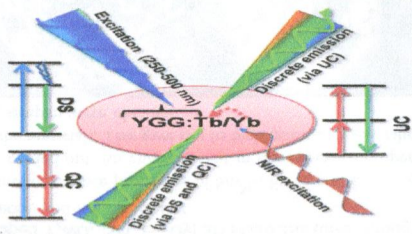

9570 dx.doi.org/10.1021/ic500866d

Kinetic Aspects for the Reduction of CO_2 and CS_2 with Mixed-Ligand Ruthenium(II) Hydride Complexes Containing Phosphine and Bipyridine

Jing Huang, Jinzhu Chen,* Hui Gao, and Limin Chen

$[Ru(H)(bpy)_2(PTA)]PF_6$ (**1a**) reacted with CO_2 and CS_2 to give the corresponding formate and dithioformate complexes, respectively. Both the insertions of CO_2 and CS_2 into the Ru−H bond of **1a** followed second-order kinetics. The second-order rate constant (k_2) of CO_2 insertion reaction varied from $(9.40 \pm 0.41) \times 10^{-4}$ M^{-1} s^{-1} in acetone to $(1.13 \pm 0.08) \times 10^{-1}$ M^{-1} s^{-1} in methanol; moreover, the $\ln(k_2)$ shows a linear relationship with the acceptor number of solvent used.

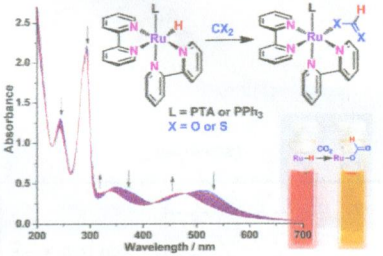

9581 dx.doi.org/10.1021/ic501004u

An Investigation of Chlorine Ligands in Transition-Metal Complexes via ^{35}Cl Solid-State NMR and Density Functional Theory Calculations

Christopher A. O'Keefe, Karen E. Johnston, Kiplangat Sutter, Jochen Autschbach, Régis Gauvin, Julien Trébosc, Laurent Delevoye, Nicolas Popoff, Mostafa Taoufik, Konstantin Oudatchin, and Robert W. Schurko*

^{35}Cl solid state NMR (SSNMR), in tandem with ^{35}Cl NQR and density functional theory calculations, was used to characterize chlorine ligands in a series of transition-metal complexes exhibiting structural motifs common to organometallic catalysts. The differentiation of the various chlorine environments was possible, and insight into the origins of the ^{35}Cl electric field gradient tensor parameters was provided. The applicability of ^{35}Cl SSNMR to the study of surface supported transition-metal complexes was demonstrated, validating the use of this technique in the characterization of heterogeneous catalysts.

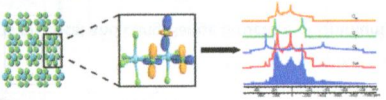

9598 dx.doi.org/10.1021/ic500959m

Synthesis, Characterization, and Reactivity of Furan- and Thiophene-Functionalized Bis(N-heterocyclic carbene) Complexes of Iron(II)

Julia Rieb, Andreas Raba, Stefan Haslinger, Manuel Kaspar, Alexander Pöthig, Mirza Cokoja, Jean-Marie Basset, and Fritz E. Kühn*

The synthesis of iron(II) complexes bearing new heteroatom-functionalized methylene-bridged bis(N-heterocyclic carbene) ligands is reported. Tetrakis(acetonitrile)-*cis*-[bis(*o*-imidazol-2-ylidenefuran)methane]iron(II) hexafluorophosphate (**2a**) and tetrakis(acetonitrile)-*cis*-[bis(*o*-imidazol-2-ylidenethiophene)methane]iron(II) hexafluorophosphate (**2b**) were obtained by aminolysis of $[Fe\{N(SiMe_3)_2\}_2(THF)]$ with furan- and thiophene-functionalized bis(imidazolium) salts in acetonitrile. Crystallization of **2a** from acetone *cis*-diacetonitriledi[bis(*o*-imidazol-2-ylidenefuran)methane]iron(II) hexafluorophosphate (**3a**). Compounds **2a** and **2b** exhibit four coordination sites occupied by solvent molecules, which are prone to ligand-exchange reactions, as demonstrated with trimethylphosphine.

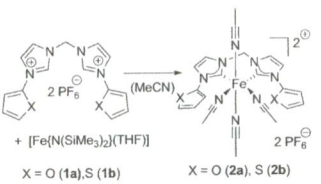

9607 S dx.doi.org/10.1021/ic501006p

Theoretical Investigation on Multiple Bonds in Terminal Actinide Nitride Complexes

Qun-Yan Wu, Cong-Zhi Wang, Jian-Hui Lan, Cheng-Liang Xiao, Xiang-Ke Wang, Yu-Liang Zhao, Zhi-Fang Chai,* and Wei-Qun Shi*

A series of actinide (An) species of L-An-N compounds have been investigated using scalar relativistic density functional theory. It is found that the bond length of terminal multiple An-N1 decreases from An = Pa to Pu, and the corresponding Mayer bond order also decreases gradually. Natural bond orbital and electron density analyses reveal that the contributions of the 6d orbital to covalency are larger in magnitude than the 5f orbital.

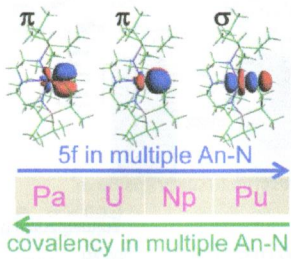

9615 S dx.doi.org/10.1021/ic501074x

Temperature- and Pressure-Induced Phase Transitions in the Metal Formate Framework of $[ND_4][Zn(DCOO)_3]$ and $[NH_4][Zn(HCOO)_3]$

Mirosław Mączka,* Paweł Kadłubański, Paulo Tarso Cavalcante Freire, Bogusław Macalik, Waldeci Paraguassu, Krysztof Hermanowicz, and Jerzy Hanuza

We report studies of temperature- and pressure-induced phase transitions in $[NH_4][Zn(HCOO)_3]$ and its deuterated analogue, which belong to metal−organic frameworks of $[NH_4][M(HCOO)_3]$ (M = divalent cation), exhibiting ferroelectric and multiferroic properties. Our data show that the temperature-induced phase transition has an order−disorder character and is governed by rotational dynamics of the ammonium cations, whereas the pressure-induced transition at about 1.1 GPa is associated with a very strong distortion of the metal formate framework.

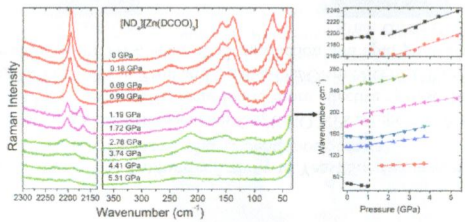

9625 dx.doi.org/10.1021/ic501118b

Anion-Dependent Assembly of Four Sensitized Near-Infrared Luminescent Heteronuclear Zn^{II}–Yb^{III} Schiff Base Complexes from a Trinuclear Zn^{II} Complex

Zhi-Peng Zheng, Yan-Jun Ou, Xu-Jia Hong, Lei-Ming Wei, Lin-Tao Wan, Wo-Hua Zhou, Qing-Guang Zhan, and Yue-Peng Cai*

Four anion-dependent 0D Zn^{II}–Yb^{III} heterometallic Schiff base complexes, $[YbZn_2L_2(OAc)_4]\cdot ClO_4$ (**2**), $YbZnL_2(NO_3)_3$ (**3**), $[(YbL)_2(H_2O)Cl(OAc)]_2\cdot[ZnCl_4]_2$ (**4**), and $YbZnL(OAc)_4$ (**5**), were assembled through central metal substitution or reconstruction from homotrinuclear Zn^{II} complex $\{[(Zn(OAc)(H_2O)L]_2Zn\}(ClO_4)_2\cdot 4H_2O$ [**1**; HL = 2-ethoxy-6-[(pyridin-2-ylmethylimino)methyl]phenol] with different $Yb^{III}X_3$ salts [X = ClO_4 (**2**), NO_3 (**3**), Cl (**4**), and OAc (**5**)], in which the Zn^{II}-sensitized near-infrared luminescent performances in the four complexes **2**–**5** are closely related to their structural models.

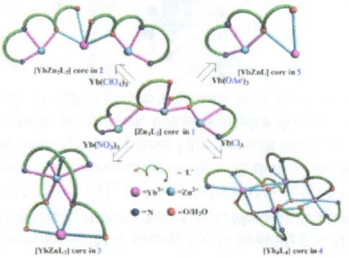

9633 dx.doi.org/10.1021/ic501134y

A 3D Oxalate-Based Network as a Precursor for the $CoMn_2O_4$ Spinel: Synthesis and Structural and Magnetic Studies

Jelena Habjanič, Marijana Jurić,* Jasminka Popović, Krešimir Molčanov, and Damir Pajić

A novel heterometallic oxalate-based compound, $\{[Co(bpy)_3][Mn_2(C_2O_4)_3]\cdot H_2O\}_n$ (**1**; bpy = 2,2′-bipyridine), made of a 3D anionic network is used as a single-source precursor for preparation of the mixed-metal oxide $CoMn_2O_4$ through its thermal decomposition. The spectroscopic, structural, and magnetic properties of this framework as well as spinel oxide obtained at 800 °C are investigated.

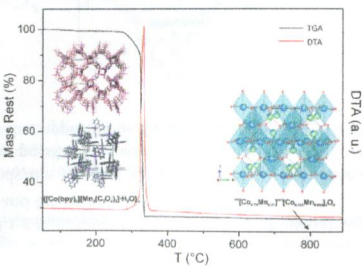

9644 S dx.doi.org/10.1021/ic501139w

Addressing the Chemical Sorcery of "GaI": Benefits of Solid-State Analysis Aiding in the Synthesis of P→Ga Coordination Compounds

Brian J. Malbrecht, Jonathan W. Dube, Mathew J. Willans, and Paul J. Ragogna*

For the first time the synthesis and convincing solid-state characterization of different phases of "GaI"—a common low-valent gallium precursor—is described. After 40 min of sonication time a gray phase with the overall formula $[Ga^0]_2[GaI_2]_2$ is produced, which quantitatively converts to a green phase with an overall formula of $[Ga^0]_2[Ga_2I_3]_2$. These gallium compounds were characterized by FT-Raman spectroscopy and powder XRD, as well as solid-state NMR and NQR spectroscopy, and also give rise to different products when treated with chelating phosphines.

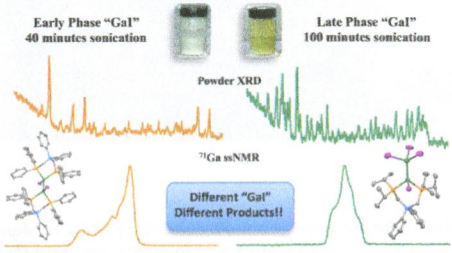

9657 dx.doi.org/10.1021/ic501143z

Selective Synthesis of Cu_2O and Cu/Cu_2O NPs: Antifungal Activity to Yeast *Saccharomyces cerevisiae* and DNA Interaction

K. Giannousi, G. Sarafidis, S. Mourdikoudis, A. Pantazaki, and C. Dendrinou-Samara*

A fungistatic and fungicidal activity of Cu_2O and heterogeneous Cu/Cu_2O NPs is reported. Nearly spherical Cu_2O@OAm and Cu_2O@Tween 20 NPs of 30 and 12 nm, respectively, were found more effective against the yeast *S. cerevisiae* than the core–shell and semishell Cu/Cu_2O@TEG NPs of 7 nm and Cu/Cu_2O@OAm NRs of 170 nm. DNA binding and degradation depend on the size and concentration of the NPs, while ROS production and lipid peroxidation were verified.

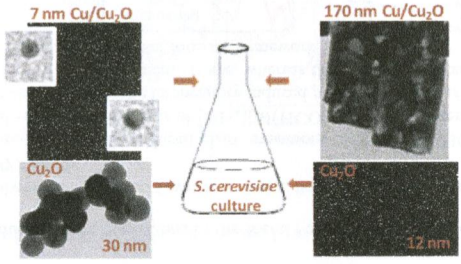

9667 S dx.doi.org/10.1021/ic501177t

Solvation Structure of a Copper(II) Ion in Protic Ionic Liquids Comprising *N*-Hexylethylenediamine

Shinobu Takemura, Sayaka Kawakami, Masafumi Harada, and Masayasu Iida*

The copper(II) ion is strongly encapsulated in the monoprotonated Hexen(Tf_2N) ionic liquid. The fine structure of the copper(II) ion in the chelating ionic liquid has been clarified in a comparison with analogous solvents. The lifetime of the copper(II) complex in the ionic liquid has been determined to be 10^{-4} s, which is much longer than that in molecular liquids.

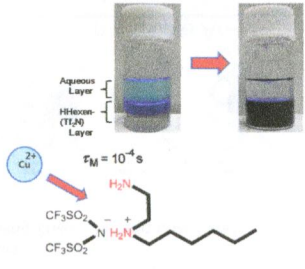

9679 S

dx.doi.org/10.1021/ic5011538

Computational Exploration of Alternative Catalysts for Olefin Purification: Cobalt and Copper Analogues Inspired by Nickel Bis(dithiolene) Electrocatalysis

Haixia Li, Edward N. Brothers,* and Michael B. Hall*

Inspired by the nickel bis(dithiolene) electrocatalytic olefin-purification cycle, computational investigations were conducted to explore alternative candidates $[M(S_2C_2(CF_3)_2)_2]^n$ (M = Co with n = 0, −1, −2, −3 and Cu with n = +1, 0, −1, −2) by using ethylene as the olefin. Thermodynamic and kinetic (transition state) results show that the cobalt complex should perform better than the nickel complex. This study could provide some guidance to the design of new catalysts to examine experimentally.

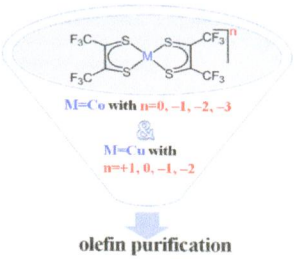

9692 S

dx.doi.org/10.1021/ic501179b

Uptake of One and Two Molecules of 1,3-Butadiene by Platinum Bis(dithiolene): A Theoretical Study

Li Dang,* Shao Fei Ni, Michael B. Hall, and Edward N. Brothers

DFT calculation was carried out to study the 1,2- and 1,4-additions of 1,3-butadiene on the ligands of $Pt(tfd)_2$ to form interligand and intraligand adducts. The possible pathways leading to different adducts in the proposed mechanisms were investigated, and the adduct selectivity that appeared in the experiment was explained.

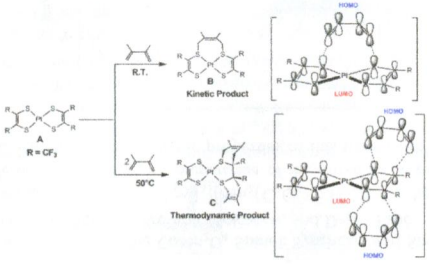

9703 S

dx.doi.org/10.1021/ic501232z

Structural Distortions in $M[E(SiMe_3)_2]_3$ Complexes (M = Group 15, f-Element; E = N, CH): Is Three a Crowd?

Nicholas C. Boyde, Stephen C. Chmely, Timothy P. Hanusa,* Arnold L. Rheingold, and William W. Brennessel

The tris(bistrimethylsilylamido) species $P[N(SiMe_3)_2]_3$ (**1**) and $As[N(SiMe_3)_2]_3$ (**2**) have been prepared through halide metathesis in high yield. Their single crystal X-ray structures, along with that of $Sb[N(SiMe_3)_2]_3$ (**3**), complete the series of structurally authenticated group 15 $M[N(SiMe_3)_2]_3$ complexes (the bismuth analogue (**4**) has been previously reported). All four complexes possess the expected pyramidal geometries, but also display distortions that are similar to those in f-element $M[(N,CH)(SiMe_3)_2]_3$ complexes, in which M···(β-Si−C) interactions have been identified.

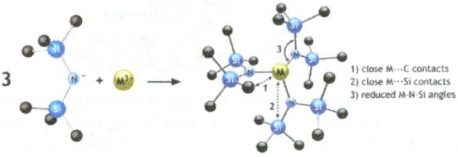

9715 dx.doi.org/10.1021/ic5012378

Revisiting the Crystal Structure of Rhombohedral Lead Metaniobate

Gerhard Henning Olsen, Magnus Helgerud Sørby, Bjørn Christian Hauback, Sverre Magnus Selbach, and Tor Grande*

The crystal structure and energetic stability of the stable rhombohedral polymorph of lead metaniobate ($PbNb_2O_6$) is re-examined by powder X-ray diffraction, powder neutron diffraction, and ab initio calculations. This structure is described by the polar space group *R*3. The crystal structure consists of edge-sharing dimers of $NbO_{6/2}$ octahedra forming layers with 6- and 3-fold rings of octahedra and lead ions in channels formed by these rings. The layers are connected by corner-sharing between octahedra.

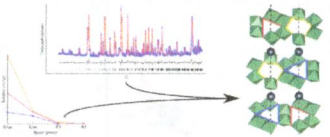

9722 dx.doi.org/10.1021/ic5012296

Synthesis and Characterization of the New Strontium Borogermanate $Sr_{3-x/2}B_{2-x}Ge_{4+x}O_{14}$ ($x = 0.32$)

Benedikt Petermüller, Lucas L. Petschnig, Klaus Wurst, Gunter Heymann, and Hubert Huppertz*

A new strontium borogermanate with the composition $Sr_{3-x/2}B_{2-x}Ge_{4+x}O_{14}$ ($x = 0.32$), being the first boron-containing member of the langasite family, was synthesized by a high-temperature solid-state reaction.

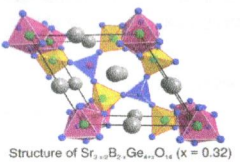

Structure of $Sr_{3-x/2}B_{2-x}Ge_{4+x}O_{14}$ ($x = 0.32$)

9729 dx.doi.org/10.1021/ic5012555

High-Pressure Raman Scattering of $CaWO_4$ Up to 46.3 GPa: Evidence of a New High-Pressure Phase

Pablo Botella, Raúl Lacomba-Perales, Daniel Errandonea,* Alain Polian, Placida Rodríguez-Hernández, and Alfonso Muñoz

The HP structural behavior of $CaWO_4$ was studied using Raman spectroscopy and *ab initio* calculations, extending the pressure range of previous studies up to 46.3 GPa. Experiments were carried out for the first time under quasi-hydrostatic conditions. The scheelite–fergusonite transition was confirmed, and a new phase transition was discovered. The structure for the HP phase is proposed and its electronic structure calculated. The pressure dependence of all Raman-active phonons is determined.

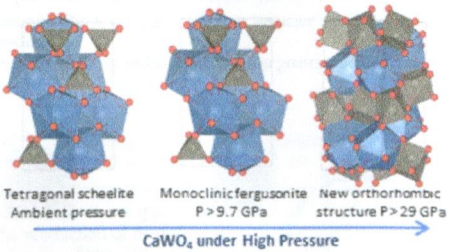

9739 S dx.doi.org/10.1021/ic501278n

Synthesis and Spectroscopy of Anionic Cyclometalated Iridium(III)-Dithiolate and -Sulfinates—Effect of Sulfur Dioxygenation on Electronic Structure and Luminescence

Van Ha Nguyen, Hui Qi Chew, Bochao Su, and John H. K. Yip*

A heteroleptic Ir^{III}(2-phenylbipyridine)$_2$dithiolate $[\mathbf{IrSS}]^-$ complex undergoes rapid dioxygenation to produce a monosulfinate complex $[\mathbf{IrSSO_2}]^-$, which can be oxidized to disulfinate complex $[\mathbf{IrSO_2SO_2}]^-$. The reaction changes electronic structure, leading to different ground states and excited states as reflected in the absorption and emission spectra of the complexes and accounted for by DFT calculations.

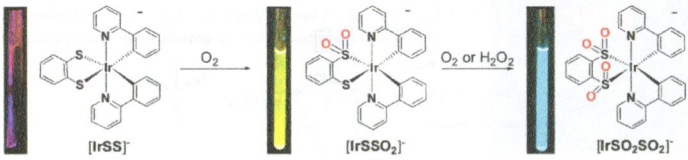

9751 S dx.doi.org/10.1021/ic501335e

Selective Sensitization of Eu(III) and Tb(III) Emission with Triarylboron-Functionalized Dipicolinic Acids

Hee-Jun Park, Soo-Byung Ko, Ian W. Wyman, and Suning Wang*

Triarylboryl-functionalized dipicolinic acids have been achieved. The T_1 energies of these new ligands were found to be highly sensitive to the nature of the aryl linker, leading to selective sensitization of Tb(III) or Eu(III) emission that can be either quenched or enhanced by the addition of fluoride ions in a reversible manner.

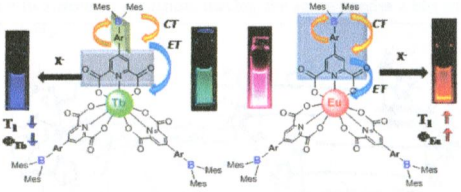

9761 S dx.doi.org/10.1021/ic501346a

Octahedral Co-Carbide Carbonyl Clusters Decorated by $[AuPPh_3]^+$ Fragments: Synthesis, Structural Isomerism, and Aurophilic Interactions of $Co_6C(CO)_{12}(AuPPh_3)_4$

Iacopo Ciabatti, Cristina Femoni, Mohammad Hayatifar, Maria Carmela Iapalucci, Andrea Ienco, Giuliano Longoni, Gabriele Manca, and Stefano Zacchini*

Octahedral Co-carbide carbonyl clusters decorated by $[AuPPh_3]^+$ fragments display different structures in the solid state as a consequence of packing forces, aurophilic as well as weak $\pi-\pi$ and $\pi-H$ interactions.

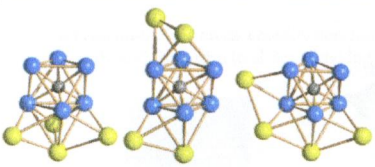

9771 S

dx.doi.org/10.1021/ic5013632

Phase Transition and Vapochromism in Molecular Assemblies of a Polymorphic Zinc(II) Schiff-Base Complex

Ivan Pietro Oliveri, Graziella Malandrino, and Santo Di Bella*

An amphiphilic Zn^{II} Schiff-base complex shows unique thermochromic and vapochromic characteristics. The dimorphism of this novel material is associated with an irreversible, thermally induced phase transition from a lamellar-to-hexagonal columnar structure, responsible for the thermochromic behavior, while vapochromism is related to the formation of 1:1 adducts upon exposure to vapors of strong Lewis bases. The chemisorption process is fast, completely reversible, reproducible, and selective for amines.

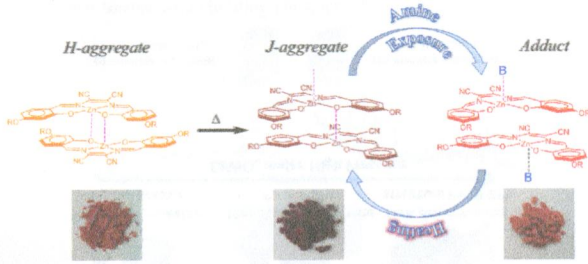

9778

dx.doi.org/10.1021/ic501366d

Quantitative Analysis of Deconvolved X-ray Absorption Near-Edge Structure Spectra: A Tool To Push the Limits of the X-ray Absorption Spectroscopy Technique

Paola D'Angelo,* Valentina Migliorati, Ingmar Persson, Giordano Mancini, and Stefano Della Longa

A new approach using a deconvolution procedure and a quantitative analysis of the X-ray absorption near-edge structure (XANES) spectra has been applied to the study of lanthanoid-containing systems. New features have emerged from the raw data that were previously hidden due to instrumental and core-hole lifetime broadening. This opens up new possibility for the XANES technique.

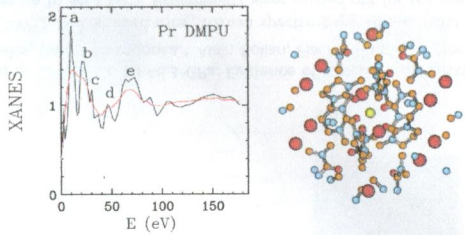

9785 S

dx.doi.org/10.1021/ic501374q

Synthesis, Structure, and Magnetic Properties of $Dy_2Co_2L_{10}(bipy)_2$ and $Ln_2Ni_2L_{10}(bipy)_2$, *Ln* = La, Gd, Tb, Dy, and Ho: Slow Magnetic Relaxation in $Dy_2Co_2L_{10}(bipy)_2$ and $Dy_2Ni_2L_{10}(bipy)_2$

Fang-Hua Zhao, Hui Li, Yun-Xia Che, Ji-Min Zheng,* Veacheslav Vieru, Liviu F. Chibotaru, Fernande Grandjean, and Gary J. Long

The single-crystal structure of the newly synthesized isomorphous $Dy_2Co_2L_{10}(bipy)_2$ and $Ln_2Ni_2L_{10}(bipy)_2$ complexes, with *Ln* = La, Gd, Tb, Dy, and Ho, reveals well-isolated, close to linear Co···Dy···Dy···Co and Ni···*Ln*···*Ln*···Ni cationic clusters. The ac magnetic susceptibility studies reveal that $Dy_2Co_2L_{10}$ $(bipy)_2$ and $Dy_2Ni_2L_{10}(bipy)_2$ exhibit slow magnetic relaxation with large effective energy barriers, U_{eff}, for the reversal of their magnetization.

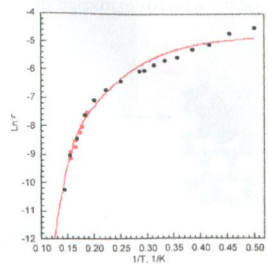

9800

Perovskite-Structure $TlMnO_3$: A New Manganite with New Properties

Wei Yi, Yu Kumagai, Nicola A. Spaldin, Yoshitaka Matsushita, Akira Sato, Igor A. Presniakov, Alexey V. Sobolev, Yana S. Glazkova, and Alexei A. Belik*

A new member of the $AMnO_3$ trivalent perovskite manganite family, $TlMnO_3$, was prepared under high-pressure and high-temperature conditions. It shows distinct structural and magnetic properties from all other $AMnO_3$ manganites. It crystallizes in a triclinically distorted structure with space group $P\bar{1}$ and exhibits fully compensated antiferromagnetic properties.

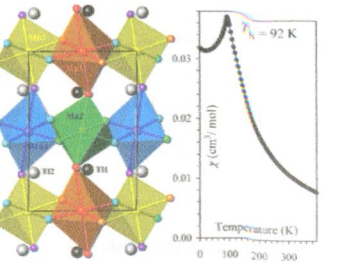

9809

dx.doi.org/10.1021/ic501402q

A Homologous Series of $[Fe(H_2Bpz_2)_2(L)]$ Spin-Crossover Complexes with Annelated Bipyridyl Co-Ligands

Rafal Kulmaczewski, Helena J. Shepherd, Oscar Cespedes, and Malcolm A. Halcrow*

Four iron(II) complexes $[Fe(H_2Bpz_2)_2(L)]$ (pz = pyrazolyl; L = dppz, or another annelated bipyridyl chelate) crystallize in different molecular stacking motifs through interdigitation of the bipyridyl ligands, often with intercalated toluene or additional uncoordinated bipyridyl. Despite these strong intermolecular interactions the compounds exhibit rather gradual thermal spin-equilibria, because most of the structural rearrangement during spin-crossover occurs at the periphery of the stacks where the crystal packing is less dense.

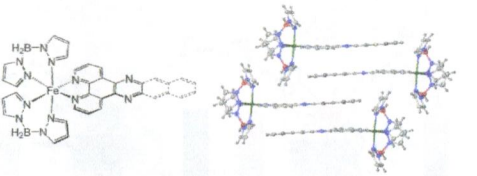

9818

dx.doi.org/10.1021/ic5014208

Preparation and Reactivity of the Versatile Uranium(IV) Imido Complexes $U(NAr)Cl_2(R_2bpy)_2$ (R = Me, ^{t}Bu) and $U(NAr)Cl_2(tppo)_3$

Robert E. Jilek, Neil C. Tomson, Ryan L. Shook, Brian L. Scott, and James M. Boncella*

Triphenylphosphine oxide and 2,2′-bipyridyl adducts of UCl_4 react with 2 equiv of various lithium anilides to afford mononuclear, monoimido U(IV) complexes in good yields. These species are shown to serve as convenient entries in complexes containing U(V) bis(imido), U(VI) bis(imido), and U(VI) oxo-imido moieties, as well as alternative U(IV) complexes resulting from halide group exchange and imido group protonolysis reactivity.

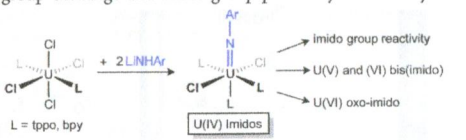

9827 S dx.doi.org/10.1021/ic501389s

Drastic Effect of Lattice Propionitrile Molecules on the Spin-Transition Temperature of a 2,2′-Dipyridylamino/s-triazine-Based Iron(II) Complex

Nanthawat Wannarit, Nassim Nassirinia, Saeid Amani, Norberto Masciocchi,* Sujittra Youngme, Olivier Roubeau,* Simon J. Teat, and Patrick Gamez*

The gradual loss of the lattice propionitrile molecules of an iron(II) compound from a 2,2′-dipyridylamino/s-triazine ligand gives rise to a clear change in its SCO properties, as evidenced by the lowering of $T_{1/2}$ by 63 K.

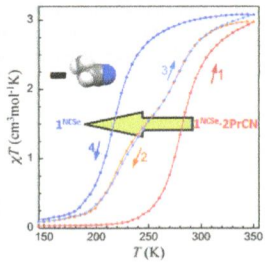

9837 S dx.doi.org/10.1021/ic501424e

Structural and Spectroscopic Characterization of Iron(II), Cobalt(II), and Nickel(II) *ortho*-Dihalophenolate Complexes: Insights into Metal−Halogen Secondary Bonding

Timothy E. Machonkin,* Monica D. Boshart, Jeremy A. Schofield, Meghan M. Rodriguez, Katarzyna Grubel, Dalia Rokhsana, William W. Brennessel, and Patrick L. Holland*

A series of six $Tp^{Ph2}ML$ complexes, where M = Fe(II), Co(II), or Ni(II) and L = 2,6-dichloro- or 2,6-dibromophenolate, was synthesized and structurally characterized. All six complexes exhibited metal−halogen secondary bonding. Variable temperature NMR and DFT calculations indicated that the secondary bonding is a weak noncovalent interaction comparable to a hydrogen bond. These results provide insight into the specificity of the enzyme PcpA for halogenated substrates and inhibitors.

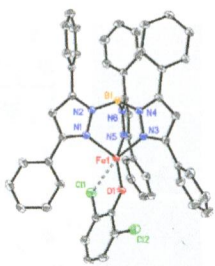

9849 S dx.doi.org/10.1021/ic501378w

Homogeneous Hydrogenation of CO_2 to Methyl Formate Utilizing Switchable Ionic Liquids

Mahendra Yadav, John C. Linehan, Abhijeet J. Karkamkar, Edwin van der Eide, and David. J. Heldebrant*

Capture of CO_2 and subsequent hydrogenation allows for base/methanol-promoted homogeneous hydrogenation of CO_2 to methyl formate. The CO_2 reacts with H_2 with no applied pressure of CO_2 in the presence of a catalyst to produce amidinium formate, then methyl formate. The production of methyl formate releases the base back into the system, thereby reducing one of the flaws of catalytic hydrogenations of CO_2: the consumption of one mole of base per mole of formate produced.

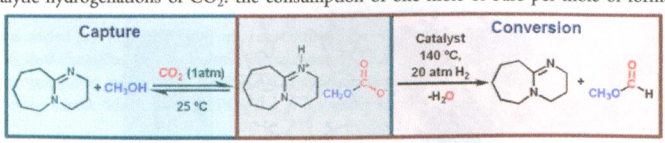

9855 dx.doi.org/10.1021/ic5014472

Synthesis and Photoluminescence Properties of an Unprecedented Phosphinine–Cu_4Br_4 Cluster

Philipp Roesch, Jörn Nitsch, Martin Lutz, Jelena Wiecko, Andreas Steffen,* and Christian Müller*

We report here on a rare example of a phosphinine-based copper cluster, which exhibits temperature-independent orange phosphorescence solely from a ^{3}XMLCT state, even at room temperature. The structural motif of a heterocubane-type $Cu_4X_4L_4$ cluster as well as its remarkable photophysical properties is so far unprecedented in phosphinine chemistry. The results presented here thus provide interesting future perspectives for the application of such aromatic phosphorus heterocycles in molecular materials sciences.

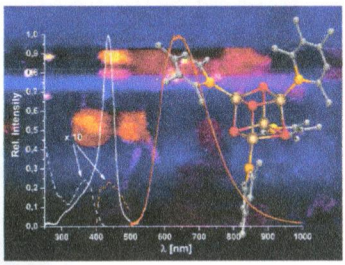

9860 dx.doi.org/10.1021/ic501440a

Light-Driven Hydrogen Production from Aqueous Protons using Molybdenum Catalysts

William T. Eckenhoff,* William W. Brennessel, and Richard Eisenberg*

A homogeneous photochemical system for hydrogen production using $[Ru(bpy)_3]^{2+}$ as light absorber, Mo bis(dithiolene) complexes as catalysts, and ascorbic acid as electron donor is described. Seven molybdenum complexes were investigated as catalysts, and turnover numbers as high as 500 were achieved. Additionally, NMR studies reveal that for the Mo catalyst isonitrile ligands dissociate after a two-electron reduction, making the active species a bis(dithiolene)molybdenum(II) species that upon addition of acid evolves H_2.

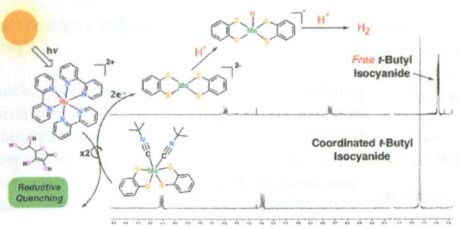

9870 dx.doi.org/10.1021/ic501459m

Synthesis and Porous Properties of Chromium Azolate Porous Coordination Polymers

Kanokwan Kongpatpanich, Satoshi Horike,* Masayuki Sugimoto, Tomohiro Fukushima, Daiki Umeyama, Yosuke Tsutsumi, and Susumu Kitagawa*

We developed a new route for synthesis of chromium-based porous coordination frameworks with azole ligands. Each Cr^{2+} and Cr^{3+} framework was prepared as single crystals, and their structural flexibility, high porosity, and reactivity to gases were characterized.

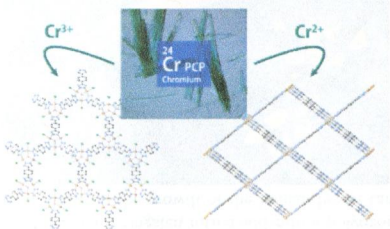

9876 dx.doi.org/10.1021/ic501482u

Trinuclear Complexes and Coordination Polymers of Redox-Active Guanidino-Functionalized Aromatic (GFA) Compounds with a Triphenylene Core

Anna Lebkücher, Christoph Wagner, Olaf Hübner, Elisabeth Kaifer, and Hans-Jörg Himmel*

By functionalization of triphenylene with six guanidino groups, new redox-active ligands were obtained. In this work, we compare the electronic properties in several trinuclear Cu^{I} and Cu^{II} complexes and show that the new ligands can be integrated into polymeric and porous structures by silver halide coordination.

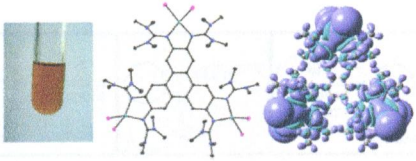

9897 dx.doi.org/10.1021/ic501529f

Probing the Role of Secondary versus Tertiary Amine Donor Ligands for Indium Catalysts in Lactide Polymerization

Kimberly M. Osten, Dinesh C. Aluthge, Brian O. Patrick, and Parisa Mehrkhodavandi*

The nature of the central amine donor may play a role in tuning the reactivity of dinuclear indium catalysts for the ring opening polymerization of lactide. Catalysts with central secondary amine donors are 2 orders of magnitude more reactive than those with central tertiary amine donors.

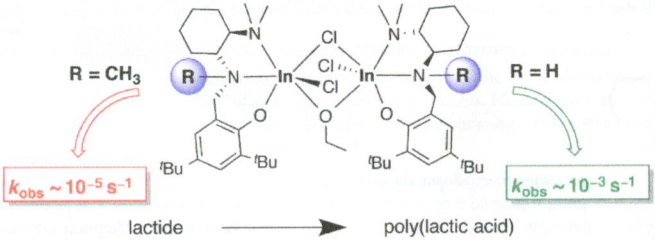

9907 dx.doi.org/10.1021/ic501574e

When the Tolman Electronic Parameter Fails: A Comparative DFT and Charge Displacement Study of $[(L)Ni(CO)_3]^{0/-}$ and $[(L)Au(CO)]^{0/+}$

Gianluca Ciancaleoni,* Nicola Scafuri, Giovanni Bistoni, Alceo Macchioni, Francesco Tarantelli, Daniele Zuccaccia, and Leonardo Belpassi*

Our theoretical study on 42 $[(L)M(CO)_n]^{\pm/0}$ complexes (M = Ni and Au) shows that in the case of nickel complexes the stretching frequency of the carbonyl (ν_{CO}) well correlates with the net donor properties of the ligand, whereas in the case of gold complexes ν_{CO} correlates with the Au → L π back-donation.

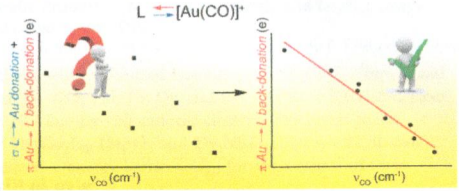

9917 S

dx.doi.org/10.1021/ic501575x

A New Nb_{28} Cluster Based on Tungstophosphate, $[\{Nb_4O_6(OH)_4\}\{Nb_6P_2W_{12}O_{61}\}_4]^{36-}$

Dongdi Zhang, Zhijie Liang, Songqiang Xie, Pengtao Ma, Chao Zhang, Jingping Wang,* and Jingyang Niu*

A nanosized 2.6 nm Nb_{28}-containing cluster, $[\{Nb_4O_6(OH)_4\}\{Nb_6P_2W_{12}O_{61}\}_4]^{44-}$ (**2**), was formed using a new synthetic strategy. Polyanion **2** represents the largest niobium/tungsten mixed-addendum polyoxometalate cluster. The preliminary in vitro assays revealed that **2a** could efficiently inhibit the growth of the human breast cancer MCF-7 cells.

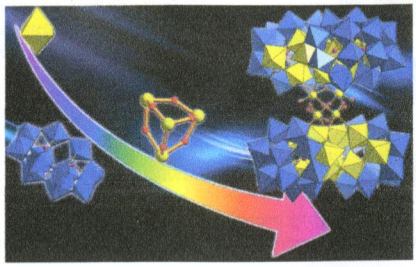

9923 S

dx.doi.org/10.1021/ic5015785

Structure and Properties of the Precursor/Successor Complex and Transition State of the $CrCl^{2+}/Cr^{2+}$ Electron Self-Exchange Reaction via the Inner-Sphere Pathway

François P. Rotzinger*

The rate constant (k) of the electron self-exchange reaction $\mathbf{Cr}Cl(OH_2)_5^{2+} + Cr(OH_2)_6^{2+} \rightarrow \mathbf{Cr}(OH_2)_6^{2+} + CrCl(OH_2)_5^{2+}$ via the inner-sphere pathway was investigated with density functional theory and wave function theory. The rate constant for the formation of the precursor complex (k_{sub}), the electronic coupling matrix element (H_{ab}), the reorganizational energy (λ), the Gibbs activation energy ($\Delta G^{\ddagger}$), and the imaginary frequency at the transition state ($\nu^{\ddagger}$) were computed with quantum-chemical methods.

$\mathbf{Cr}Cl(OH_2)_5^{2+} + Cr(OH_2)_6^{2+} \xrightleftharpoons{k} \mathbf{Cr}(OH_2)_6^{2+} + CrCl(OH_2)_5^{2+}$

$k_{et} = \Gamma_n \nu_n \kappa_{et} e^{-\Delta G^{\ddagger}/RT}$

$k = K_A k_{et}$

$k_{et} = 10-330\ s^{-1}$ at 0°C

$k = 0.3-12\ M^{-1}s^{-1}$ at 0°C and $I = 1$ M

$k(exp) = 8.3\pm2.0,\ 9.1\pm1.0\ M^{-1}s^{-1}$ at 0°C and $I = 1$ M

9932 S

dx.doi.org/10.1021/ic501581c

Framework Complexes of Group 2 Metals Organized by Homochiral Rods and $\pi\cdots\pi$ Stacking Forces: A Breathing Supramolecular MOF

Daniel L. Reger,* Andrew Leitner, Perry J. Pellechia, and Mark D. Smith

Enantiopure carboxylate ligands containing a 1,8-naphthalimide ring $\pi\cdots\pi$ stacking supramolecular tecton form Ca^{2+} and Sr^{2+} complexes with solid-state structures based on homochiral rod SBU central cores built into supramolecular MOFs by $\pi\cdots\pi$ stacking interactions between rings of adjacent rods. The supramolecular organization imparts flexibility such that these solids can undergo reversible, single-crystal to single-crystal transformations, where 1D open channels filled with water solvent close when dehydrated under vacuum and reopen when rehydrated in moist air.

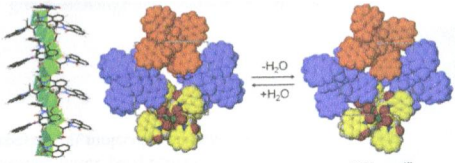

9946 dx.doi.org/10.1021/ic501704g

Cooperative Metal–Ligand Assisted *E/Z* Isomerization and Cyano Activation at Cu^{II} and Co^{II} Complexes of Arylhydrazones of Active Methylene Nitriles

Kamran T. Mahmudov,* Maximilian N. Kopylovich, Alessandra Sabbatini, Michael G. B. Drew,* Luísa M. D. R. S. Martins, Claudio Pettinari, and Armando J. L. Pombeiro*

A one-pot activation of nitrile groups in different molecules (2-cyanopyridine and arylhydrazone of active methylene nitrile) is achieved by cooperation of resonance-assisted hydrogen bonding (RAHB) and coordination in the syntheses of copper(II) complexes. *E/Z* isomerization of hydrazones is induced by the cooperative action of a metal ion and an auxiliary ligand.

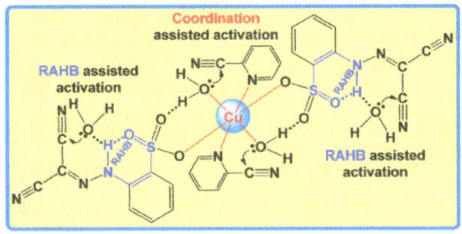

9959 dx.doi.org/10.1021/ic501733z

Crystal Growth and Characterization of the Narrow-Band-Gap Semiconductors $OsPn_2$ (Pn = P, As, Sb)

Daniel E. Bugaris, Christos D. Malliakas, Daniel P. Shoemaker, Dat T. Do, Duck Young Chung, Subhendra D. Mahanti, and Mercouri G. Kanatzidis*

Using metal fluxes, crystals of the marcasite-type binary osmium dipnictides $OsPn_2$ (Pn = P, As, Sb) have been grown for the first time. Optical-band-gap and charge-transport measurements indicate that these materials are narrow-band-gap semiconductors with electrons acting as charge carriers in nominally undoped OsP_2 and $OsSb_2$, but holes are the dominant charge carriers in $OsAs_2$. Electronic band structure and thermopower calculations agree with the experimental results.

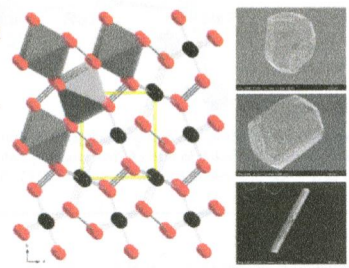

9969 dx.doi.org/10.1021/ic501781h

The Synthesis and Characterization of Four New Uranium(IV) Chlorophosphates: $UCl_4(POCl_3)$, $[U_2Cl_9][PCl_4]$, $UCl_3(PO_2Cl_2)$, and $U_2Cl_8(POCl_3)$

Matthew D. Ward, Ian Y. Chan, Sébastien Lebègue, and James A. Ibers*

The new uranium(IV) chlorophosphate compounds $UCl_4(POCl_3)$ and $[U_2Cl_9][PCl_4]$ have been synthesized by the solid-state reactions of U, P_2O_5, and PCl_5 at 648 K, and $UCl_3(PO_2Cl_2)$ and $U_2Cl_8(POCl_3)$ have been synthesized at 648 K with the same reactants plus added S. Their structures are, respectively, chainlike, a simple salt, three-dimensional, and sheetlike. From ab initio calculations $U_2Cl_8(POCl_3)$ and $UCl_3(PO_2Cl_2)$ are ferromagnetic, whereas $UCl_4(POCl_3)$ is antiferromagnetic. $U_2Cl_8(POCl_3)$ is a strong metal, whereas $UCl_3(PO_2Cl_2)$ is a weaker metal.

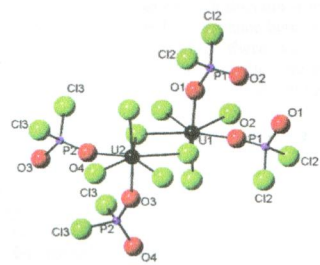

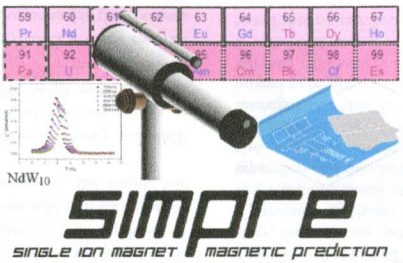

Additions and Corrections

(S) Supporting Information available via online article